Vector-Controlled Induction Motor Drive with Minimal Number of Sensors

Evgenije M. Adžić, Vlado B. Porobić, Marko S. Vekić, Zoran R. Ivanović, and Vladimir A. Katić

***Abstract*—This paper proposes an improved and robust induction motor drive control method which uses minimal number of sensors, providing only dc-link current measurement as a feedback signal. The proposed dc-link current sampling scheme and modified asymmetrical PWM pattern cancel characteristic waveform errors which exist in all three reconstructed line currents. In that way, proposed method is suitable for high-quality and high-performance drives. Comparison between conventional and proposed current reconstruction method is performed using hardware-in-the-loop (HIL) test platform and digital signal processor (DSP).**

***Index Terms*—Induction motor drive, Vector control, Sensorless control, Single current sensor.**

Original Research Paper
DOI: 10.7251/ELS1519021A

I. Introduction

CONTROLLED induction motor drives are main driving force behind all automation systems in industry. They are used in a wide range of industry applications where they significantly contribute to improved efficiency and reliability of automation processes [1]. Due to economical and reliability reasons most automation systems use induction motor drives where motor torque and speed are controlled without shaft-sensor [2]. Speed information is then determined indirectly, by measuring terminal currents and voltages [2-5]. Elimination of shaft-sensor not only reduces cost of the drive, but it also significantly increases whole system reliability. This is especially important in high-power range applications. Industry trends to provide more robust and reliable drives operation imposed necessity for drives with minimal number of sensors.

This paper proposes solution in the field of induction motor control, case where number of sensors is reduced to minimum. Only one sensor which measures the dc-link current of the converter is used. Control algorithm includes method for motor terminal current reconstruction in a way to achieve motor current and speed control. Analysis of recent relevant literature, confirms that most of the problems are recognized and solved in a way which allows their application in low-performance drives [6]-[10]. In this situation, authors usually do not consider quality and performance of implemented control algorithms.

Quality of controller is of major importance in general purpose applications having in mind their wide distribution and energy savings that can be achieved, while dynamic performances are usually put in the background. Recent developments in the electrical vehicle industry, has discovered a need to reduce the number of sensors to minimum, i.e. only one current sensor in the converter dc-link [11]. In that way, current reconstruction method becomes important also in high-performance applications. Priority in designing high-performance drives is not the cost of the drive, but accomplishing a highly accurate, stable and fast response.

Application of the current reconstruction method in a vector controlled induction motor drives proves to be significantly lower in quality and performances compared to drives using direct line current measurement. This is mainly consequence of the usual inaccuracy in reconstructed current waveforms, which is explained in details in [12]. Application of the conventional current reconstruction mechanism with two dc-link current samples in different time instants during the same switching period in combination with PWM current ripple generates error reflected in abrupt changes in reconstructed line current waveforms. This error reflects further in dq-current components in vector control algorithm, which can be observed in increased torque and speed oscillations. Moreover, in shaft-sensorless drives, accuracy in estimated speed is significantly reduced. Stability is seriously jeopardized in situations when current and speed controllers are tuned in optimal way characteristic for high-performance drives.

Conventional approach to overcome this problem employs low-pass current filters in control structure. This paper presents original solution for conventional current reconstruction method improvement, which avoids dynamic reduction, but in the same time eliminates the error and contributes to better control characteristics.

Manuscript received 21 October 2014. Received in revised form 15 June 2015. Accepted for publication 18 June 2015.

This work was financially supported by the Ministry of Education and Science of Republic of Serbia (project no. III 42004) and by the Provincial Secretariat for Science and Technological Development of AP Vojvodina (contract no. 114-451-3508/2013-04).

E. M. Adžić, V. B. Porobić, Marko S. Vekić, Zoran R. Ivanović and V. A. Katić are with the Faculty of Technical Sciences, University of Novi Sad, Serbia (phone: +381214852556, fax: +381214750572, e-mails: evgenije@uns.ac.rs, poroba@uns.ac.rs, vekmar@uns.ac.rs, zorani@uns.ac.rs, katav@uns.ac.rs).

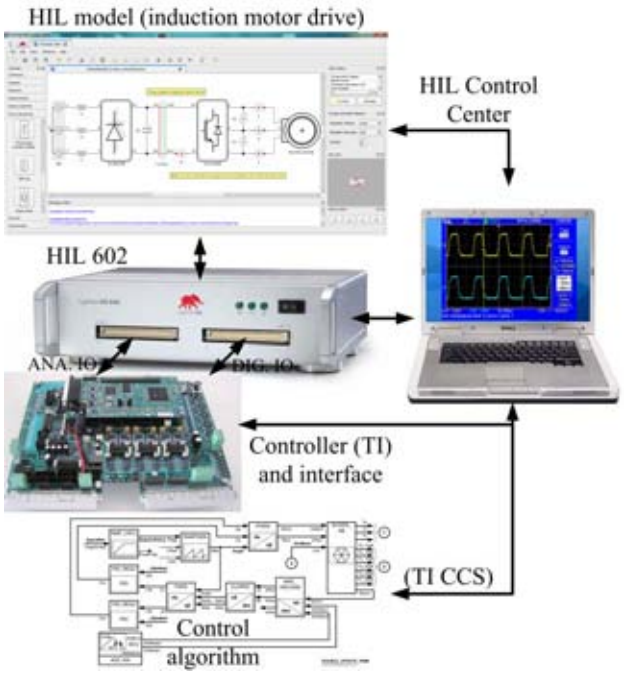

Fig. 1. Block diagram of experimental setup used for control algorithm verification.

II. Description of Experimental Setup

In order to validate effectiveness and reliability of the proposed current reconstruction method, hardware-in-the-loop (HIL) emulator was used for representing the power stage of induction motor drive. The core of the HIL platform is programmable FPGA based processor dedicated for processing power electronics circuits, with fast analog/digital input/output interface and supporting software tool-chain [13]. Beside schematic configurator and compiler, software tool-chain includes oscilloscope function for observing desired system variables and flexible debugging of the connected controller.

This approach provides real-time execution with *0,5 μs* emulation time-step and digital signals (e.g. PWM) sampling period of *20 ns* for more accurate system emulation. This feature allows the connection of real hardware controller with PWM frequency up to *100 kHz*. Controller interfaced with the HIL system is based on TMS320F2812 digital-signal processor. In all performed experiments, PWM frequency was set to *2 kHz*. Fig. 1 shows the experimental setup used for evaluation of the induction motor drive with minimal number of sensors. Motor nominal data and parameters of the related equivalent scheme are given in Table I.

TABLE I
Tested Motor Data

Symbol	Quantity	Value
P_n	Nominal power	1,1 kW
p	Number of poles	4
f_n	Nominal frequency	50 Hz
n_n	Nominal speed	1410 rpm
U_n	Nominal voltage	380 V
I_n	Nominal current	2,9 A
	Winding connection	Y (star)
J	Moment of inertia	0,00247 kgm^2
R_s	Stator resistance	9,137 Ω
R_r	Rotor resistance	6,422 Ω
$L_{\gamma r}$	Stator leakage inductance	18,89 mH
$L_{\gamma s}$	Rotor leakage inductance	17,28 mH
L_m	Magnetizing inductance	320,3 mH

III. Vector Control with the Measurement of Line Current and Speed

A. Rotor-flux oriented sensored control structure

In the early stages of the control algorithm development, current and speed controllers are set in the framework of conventional rotor-flux oriented vector control structure using directly line current and speed sensor information. This approach defines relevant framework for testing and comparison of proposed algorithm with only one dc-link sensor in a feedback path. In this stage, control algorithm uses measured line current and rotor speed as depicted in Fig. 2. Core of the control algorithm represents the flux model (*FLUX_MOD*) which is used to estimate the values of rotor flux angle (*Theta*) from the stator current vector components (*IDs* and *IQs*) and from the measured speed (*Wr*) [14].

B. Stator current controller tuning

PI current controllers for d- and q-axes are tuned using Dahlin's algorithm [15] which defines fast aperiodical step response of controlled current components, *IDs* and *IQs*, i.e. motor flux and torque. A proportional and integral gain for current controllers in discrete domain are:

$$K_{pi} = \frac{1 - e^{-\lambda T_i}}{K_{it}\left(e^{\frac{T_i}{T_\sigma}} - 1\right)\left(1 + \left(1 - e^{-\lambda T_i}\right)\right)}$$
$$K_{ii} = K_{pi}\left(e^{\frac{T_i}{T_\sigma}} - 1\right) \quad (1)$$

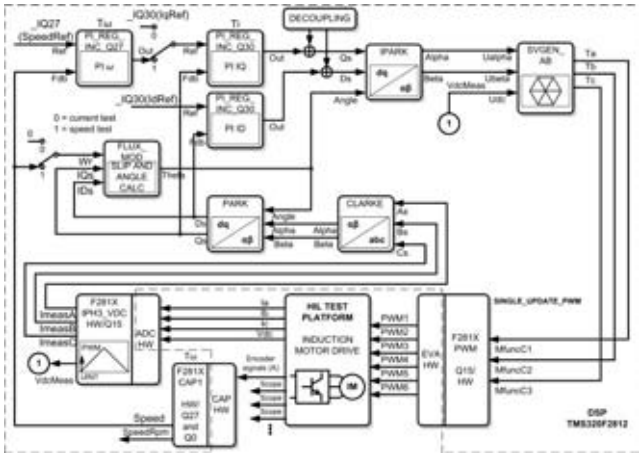

Fig. 2. DSP implementation of classical structure of rotor-flux oriented control for induction motor drive.

In Eq. 1 parameter λ defines desired dynamic of aperiodical step response, T_i represent current loop sampling period, and K_{it} is total gain in a direct path of current control loop. Total gain K_{it} equals:

$$K_{it} = \frac{u_{dc}}{\sqrt{3}} \frac{1}{R_s} \frac{1}{I_b} \tag{2}$$

where are: u_{dc} – dc-link voltage, R_s – stator winding resistance, and I_b – selected current base value. Independent design of current and speed controller is enabled by selecting the parameter λ to satisfy the condition:

$$\frac{1}{\lambda} \leq \frac{T_\omega}{5} \tag{3}$$

where T_ω represents the speed control loop sampling period. Used values for current controllers in d- and q-axes are given in Appendix section.

Dynamic response of stator current controller is given in Fig. 3. where it can be noticed that d-axis reference current was maintained on the constant value, i.e. i_d^{REF}*=0,32 p.u.*, while q-axis reference current was periodically step-changed between values *0* and *0,48 p.u.* d- and q-current references, i_d^{REF}*=0,32 p.u.* and i_q^{REF}*=0,48 p.u.*, together defines nominal current amplitude for considered motor. Fig. 3 proves that aperiodical response, without overshoot, was achieved with settling time of *19 ms* which is approximately equal to expected value of $5/\lambda$*=16,7 ms*. Fig. 4 shows corresponding response of motor line currents and electromagnetic torque. For rotor flux value defined with i_d^{REF}*=0,32 p.u.* and i_q^{REF}*=0,48 p.u.* motor develops nominal electromagnetic torque T_{en} *= 7,45 Nm* in steady-state. Torque oscillations around *4,7%*·T_{en} are consequence of PWM current.

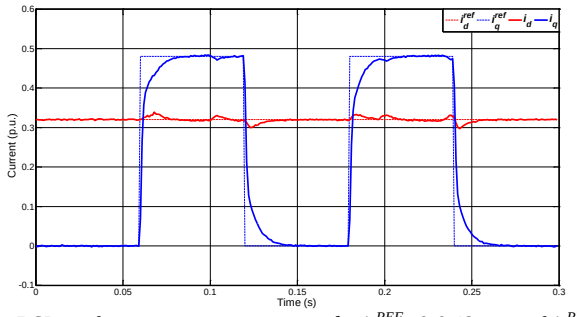

Fig. 3. DSP results: q-current step response for i_q^{REF}*=0-0,48 p.u.* and i_d^{REF} *= 0,32 p.u.*

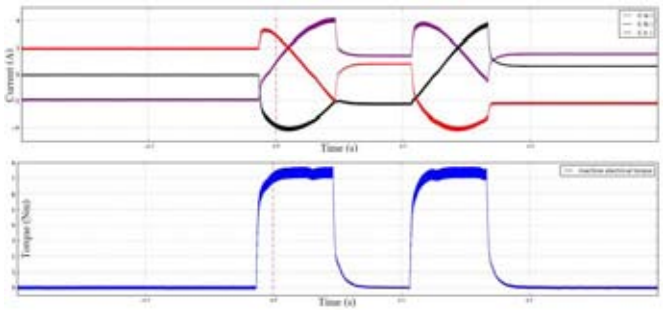

Fig. 4. HIL results: corresponding line current and electromagnetic torque response for i_q^{REF}*=0-0,48 p.u.* and i_d^{REF}*=0,32 p.u.*

Designed current controllers are used for all other experiments throughout this paper.

C. Rotor speed controller tuning

Speed controller parameters are selected in a way to obtain fast aperiodical step response. Detailed design procedure, suggested for high-performance motor drives in [16], gives following proportional and integral gains for speed controller:

$$K_{p\omega} = 0{,}2027 \frac{2J}{T_\omega} \frac{\omega_b}{K_m}$$

$$K_{i\omega} = 0{,}03512 \frac{2J}{T_\omega} \frac{\omega_b}{K_m} \tag{4}$$

In Eq. 4 J represents motor moment of inertia, ω_b is adopted base value for angular frequency, and K_m is the gain in the direct path of speed control loop model obtained from the torque equation of vector-controlled induction motor:

$$K_m = \frac{3}{2} p \frac{{L_m}^2}{L_r} i_{sd} I_b \tag{5}$$

Used parameters of speed controller are given in the Appendix. Fig. 5 shows dynamic speed response after setting step reference value ω_r^{REF} *= 0,1 – 0,4 p.u.* (*300 – 1200 rpm*). Motor was loaded with *20%* of rated torque *1,5 Nm*. Recorded HIL results in the same conditions are shown in Fig. 6. It could be noticed that speed has aperiodical transient response with settling time *0,2 s*, as expected for optimal method and parameters given with Eq. 4. Current response in field coordinates in the Fig. 5, proves that decoupled control of motor flux and torque was successfully achieved. Designed speed controller is used for all other experiments in the paper.

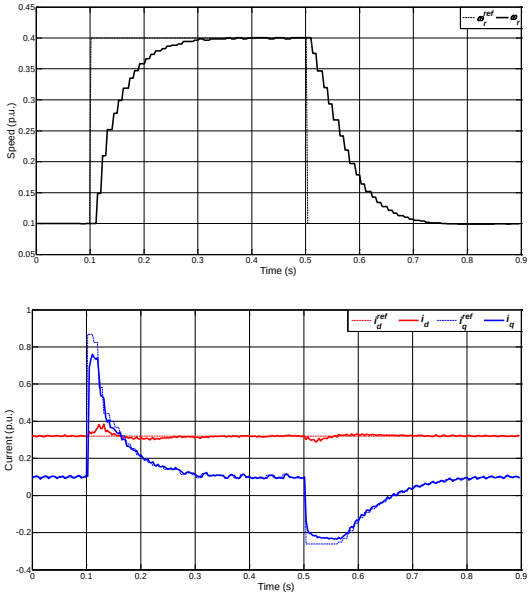

Fig. 5. DSP results: motor speed and dq-currents response for step reference ω_r^{REF} *= 0,1 / 0,4 p.u.*

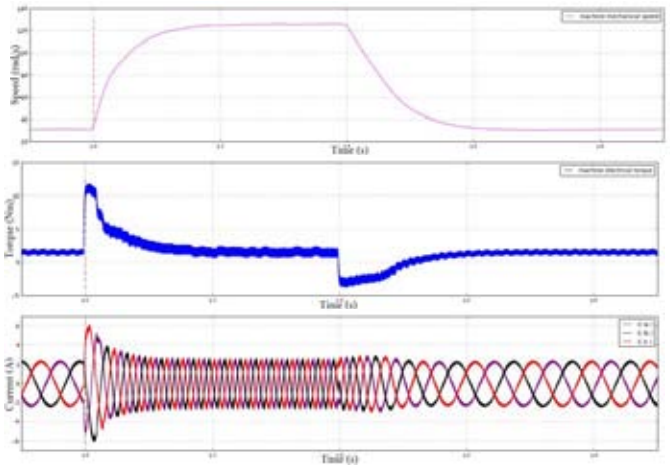

Fig. 6. HIL results: corresponding motor speed, electromagnetic torque and stator currents step response for ω_r^{REF}=0,1-0,4 p.u.

IV. Shaft-Sensorless Vector Control with Line Current Measurement

A. Rotor-flux oriented sensorless control structure

In a base speed region rotor-flux oriented vector control without speed sensor shows better performance comparing to the orientation towards stator flux vector [14]. Taking this into account and due to easier integration of sensorless control algorithm in previously described control structure, this paper uses sensorless rotor flux oriented control structure shown in Fig. 7. This fact also facilitates comparison analysis between implemented sensored and sensorless algorithms. Open-loop rotor speed estimation (*SPEED_EST*) with advanced rotor flux vector estimation (*FLUX_EST*) has been applied.

B. Estimation of rotor flux components

Regarding selected reference frame, the flux vector components are firstly calculated in term of stator coordinates, and in second step magnitude and phase angle are derived in field orientated coordinates.

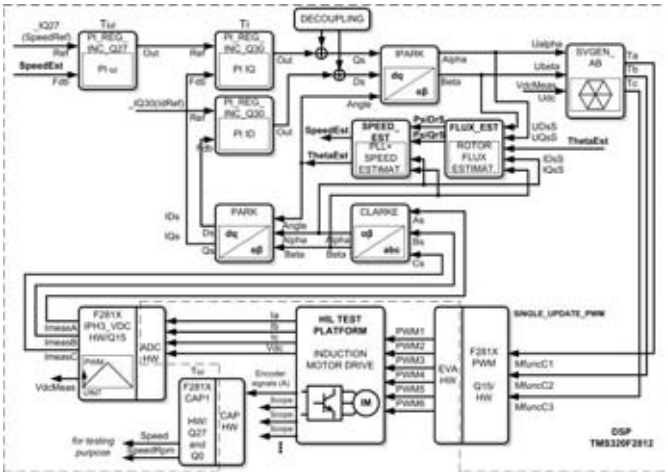

Fig. 7. DSP implementation of rotor-flux oriented sensorless control structure for induction motor drive, with advanced rotor flux estimation (*FLUX_EST*) and open-loop rotor speed estimation (*SPEED_EST*).

Used flux estimator belongs to the class of complex and advanced estimators covering wide range of speed (Fig. 8). Basically, it consists of two models: simple i_s – ω_r open-loop current model defined in field coordinates which has to provide correct estimation in the low speed range, and adaptive u_s – i_s model obtained in stator coordinates for precise estimation in wide speed range [14, 17]. Rotor flux i_s-ω_r current model (superscript i) could be derived based on motor rotor voltage and flux linkage equations in the rotor-field orientated reference frame, where stator current is used as input variable:

$$\frac{d\psi_{rd}^{i}}{dt} = \frac{L_m}{T_r} i_{sd} - \frac{1}{T_r}\psi_{rd}^{i}$$
$$\psi_{rq}^{i} = 0 \tag{6}$$

Determined rotor flux components has to be transformed in stationary reference frame with inverse Park transformation, to perform correction of adaptive rotor flux voltage model derived in stator coordinates, as depicted in Fig. 8. Stator flux components are then calculated based on the motor stator flux linkage equations:

$$\psi_{s\alpha}^{i} = \frac{L_m}{L_r}\psi_{r\alpha}^{i} + L_\sigma i_{s\alpha}$$
$$\psi_{s\beta}^{i} = \frac{L_m}{L_r}\psi_{r\beta}^{i} + L_\sigma i_{s\beta} \tag{7}$$

where L_σ represents stator leakage inductance.

Voltage model of rotor flux estimator is based on stator voltage equations in stationary reference frame, where stator flux is simply obtained by integration of stator winding induced electromotive force. Input variables are stator voltages and currents. Stator voltages are not directly measured. They are estimated based on measured dc-link voltage and inverter switching states. Dead-time and switching components for voltage drop compensation scheme is applied. Due to pure integration of input variables, stator voltage and current, compensation terms are included in the model to provide adaptive mechanism for elimination of offset error, erroneous initial values or their disturbances. Adaptive stator flux model is given (superscript u):

$$\psi_{s\alpha}^{u} = \int \left(u_{s\alpha} - R_s i_{s\alpha} - u_\alpha^{comp}\right) dt$$
$$\psi_{s\beta}^{u} = \int \left(u_{s\beta} - R_s i_{s\beta} - u_\beta^{comp}\right) dt \tag{8}$$

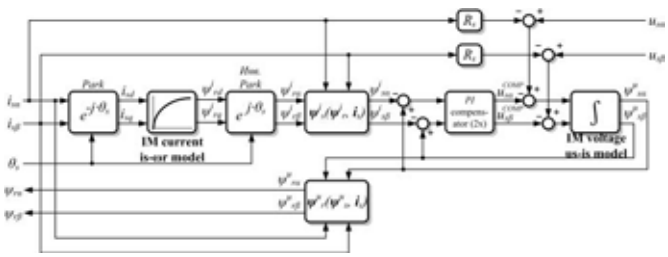

Fig. 8. Block diagram of algorithm for rotor flux estimation.

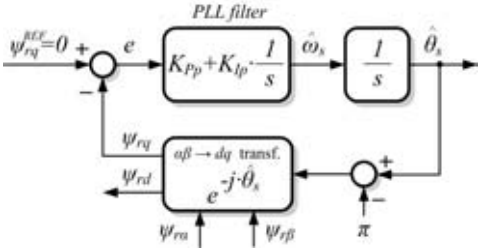

Fig. 9. Block diagram of PLL algorithm implemented in dq-reference frame.

Compensation terms, u_α^{comp} and u_β^{comp}, represents outputs of PI controllers that eliminates the error between the ideal current model (Eq. 6) and voltage model of stator flux:

$$u_\alpha^{comp} = K_{pf}\left(\psi_{s\alpha}^u - \psi_{s\alpha}^i\right) + K_{if}\int\left(\psi_{s\alpha}^u - \psi_{s\alpha}^i\right)dt$$
$$u_\beta^{comp} = K_{pf}\left(\psi_{s\beta}^u - \psi_{s\beta}^i\right) + K_{if}\int\left(\psi_{s\beta}^u - \psi_{s\beta}^i\right)dt \quad (9)$$

Parameters K_{pf} and K_{if} are determined in the way that current model in adaptive stator flux model dominates in the low speed range, while voltage model prevails in the high-speed range [17]. Finally, outputs of the rotor flux estimator are rotor flux components obtained from motor flux linkage equations in stationary reference frame:

$$\psi_{r\alpha}^u = \frac{L_r}{L_m}\left(\psi_{s\alpha}^u - L_\sigma i_{s\alpha}\right)$$
$$\psi_{r\beta}^u = \frac{L_r}{L_m}\left(\psi_{s\beta}^u - L_\sigma i_{s\beta}\right) \quad (10)$$

Determined rotor flux components are later used for rotor flux vector position and rotor speed estimation.

C. Rotor flux vector phase angle estimation

Exact determination of rotor flux vector phase angle, i.e. its position, is necessary for correct and proper transformation of all quantities in the field-rotating reference frame in which control algorithm is implemented. Solution of this problem mainly determines quality of the whole control structure, because error in the phase angle has significant negative influence on the independent control of dq-currents [14].

One of the standard and advanced methods for flux phase angle estimation represents Phase-Locked-Loop (PLL) structure implemented in rotating reference frame [18]. Block diagram of PLL algorithm used in this paper is shown in the Fig. 9. As input values, PLL uses previously determined rotor flux components in stationary reference frame. Rotor flux components are transformed in dq rotating reference frame using estimated rotor flux phase angle at the PLL output.

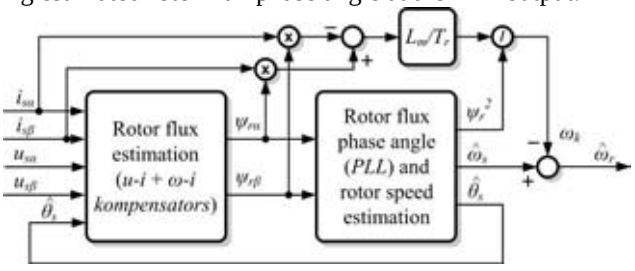

Fig. 10. Open-loop direct rotor speed estimation based on rotor flux vector.

Error signal is formed as a difference between rotor flux q-axis component reference set to 0 and obtained rotor flux q-axis component after transformation. This actually results in rotor flux vector tracking, i.e. in equalization of estimated and actual rotor flux phase angles. PLL filter in the form of PI compensator leads to reducing of error signal to zero value, also for flux frequency step changes. Parameters of PLL filter are selected in a way to provide aperiodical phase angle response with desired bandwidth of PLL control loop ω_{bw} [19]:

$$K_{pp} = \frac{\sqrt{2}}{f_b}\omega_{bw}$$
$$K_{ip} = \frac{1}{2f_b}{\omega_{bw}}^2 \quad (11)$$
$$K_{ip}^z = K_{ip}T_p$$

Integral gain of the PLL filter K_{ip} has to be multiplied with PLL sampling loop to obtain corresponding gain K_{ip}^z for digital implementation. Selected values used throughout all the experiments in the paper are given in Table II.

D. Open-loop estimation of rotor speed

Rotor flux angular frequency represents the first derivate of rotor flux phase angle, so it yields:

$$\omega_s = \frac{d\theta_s}{dt} = \frac{d\left(\operatorname{arctg}\left(\frac{\psi_{r\beta}}{\psi_{r\alpha}}\right)\right)}{dt} = \frac{\psi_{r\alpha}\frac{d\psi_{r\beta}}{dt} - \psi_{r\beta}\frac{d\psi_{r\alpha}}{dt}}{\psi_{r\alpha}^2} \quad (12)$$

By eliminating rotor currents from the rotor flux linkage equations in the induction motor model [14], and based on voltage equations for rotor winding in stationary reference frame, rotor flux angular frequency could be obtained in the following form:

$$\omega_s = \omega_r + \frac{1}{\psi_r^2}\frac{L_m}{T_r}\left(\psi_{r\alpha}i_{s\beta} - \psi_{r\beta}i_{s\alpha}\right) = \omega_r + \omega_k \quad (13)$$

ω_k represents slip frequency which is directly proportional to motor electromagnetic torque with assumption that rotor flux is maintained on constant value. Rotor speed can be estimated with:

$$\omega_r = \omega_s - \omega_k = \omega_s - \frac{1}{\psi_r^2}\frac{L_m}{T_r}\left(\psi_{r\alpha}i_{s\beta} - \psi_{r\beta}i_{s\alpha}\right) \quad (14)$$

Block diagram of implemented rotor speed estimator is shown in the Fig. 10.

E. Test results

Here are presented the main test results when feedback is closed using estimated speed and the concept described in previous chapter. Figs. 11 and 12, show motor speed, electromagnetic torque and stator current response under the same circumstances in which speed loop was closed with the measured rotor speed. Speed reference is changed in step manner between values ω_r^{REF} = *0,1 – 0,4 p.u.* with motor load

of *1,5 Nm*.

Fig. 11 shows relative values of control variables recorded in the DSP. Average speed settling time of *0,14 s* is not exact the same, but it is very close to the case when speed was measured. q-component of the stator current and corresponding torque oscillations are slightly increased, due to the PLL filter and rotor flux PI compensators in the control feedback path. Moreover, motor line currents are sinusoidal without significant distortion, similar to the case when speed loop was closed using measured rotor speed (Fig. 12).

V. Sensorless Vector Control with Conventional Current Reconstruction Method

A. Conventional current reconstruction method

Constant requirements for reducing cost and increasing reliability of the motor drives lead to the series of research with the aim to reduce number of sensors to its essential minimum. Research in the field proved that it is possible to reduce number of current sensors in three-phase AC drives to only one sensor in the dc-link. Block diagram of such drive is shown in the Fig. 13. Among previously described control structures, a core of the control scheme is block with motor phase currents reconstruction (*IABC_RECONS*) and modified switching modulator (*SVGEN_AB2*) with the task to support critical cases in reconstruction mechanism.

Due to the topology of three-phase inverter and selected switching modulation (SVPWM), it is possible to reconstruct motor phase currents from measured dc-link current [20]. In each switching period, dc-link current includes information about two motor line currents while remaining third current could be reconstructed taking into account that sum of the line currents is equal to zero. Fig. 14 shows an example and details of conventional current reconstruction principle, where switching PWM signals *A*, *B* and *C* for upper inverter switches are arranged defining output voltage vector in the first SVPWM sector. Two dc-link samples are taken in strategic moments (*SAMP1* and *SAMP2*) precisely synchronized regarding the middle of switching PWM period (*TRIG*) and according to the beginning of the active voltage vectors, as shown in Fig. 14. Here, current sample (i_h) during active voltage vector with only one upper switch turned-on is equal to phase current i_a, while current sample ($-i_l$) during active voltage vector with two upper switches turned-on is equal to inverted value of motor phase current i_c. Similar analysis could be performed for other SVPWM sectors that yield to complete current reconstruction algorithm [20].

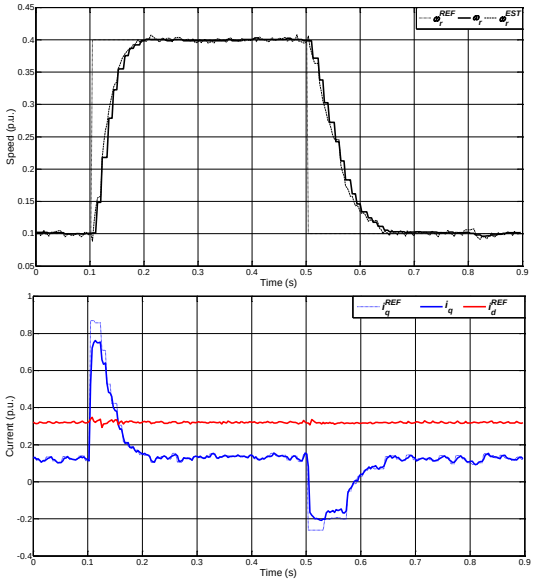

Fig. 11. DSP results: motor speed and dq-currents response for step reference ω_r^{REF} = *0,1 / 0,4 p.u.* – sensorless case with current measurement.

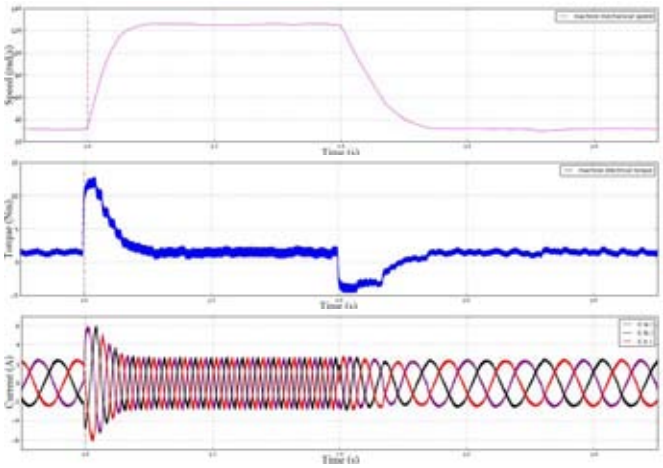

Fig. 12. HIL results: motor speed, torque and stator currents step response for ω_r^{REF}=*0,1-0,4 p.u.* – sensorless case with current measurement.

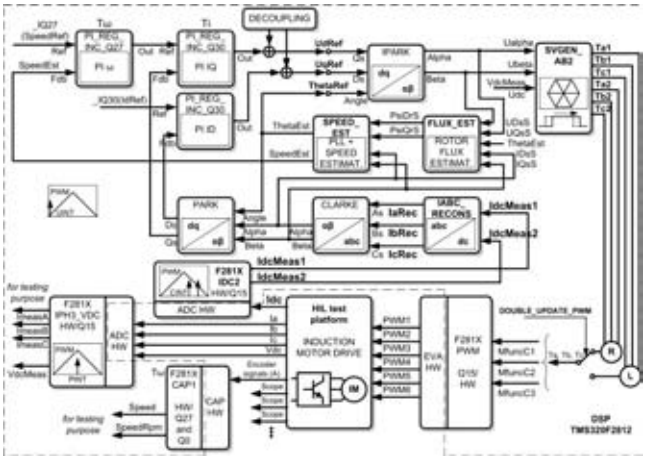

Fig. 13. DSP implementation of sensorless control structure for induction motor drive, with conventional current reconstruction algorithm (*FLUX_EST*) and modified SVPWM modulation (*SPEED_EST*).

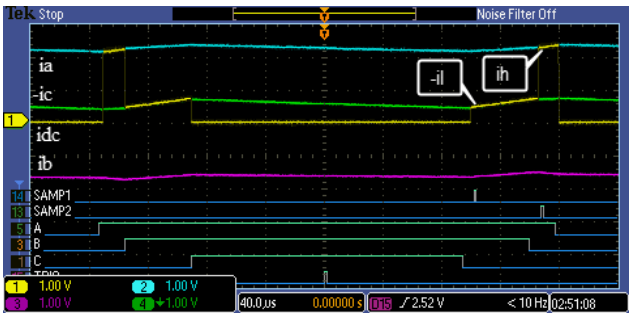

Fig. 14. Conventional dc-link current sampling and line current reconstruction method – example for first SVPWM sector.

B. *Modified SVPWM method*

Practical problems with dc-link current sampling, occur when switching PWM period contains narrow active voltage vectors. First critical case represents a situation where the reference voltage vector passes between SVPWM sectors, and when duty cycles values for two inverter legs are almost equal. Fig. 15a shows example of this case, when voltage vector passes between the first and the second sector and when it is possible to reconstruct only one line current, $-i_c$. Line current i_a is unobservable. This is always the case in normal operation due to the reference vector rotation, and it is independent on modulation index value. Second critical situation occurs in the case of small reference amplitudes of output voltage vector, i.e. in the case of small modulation index. This is a usual situation in the case of low reference speed and low motor load torque. PWM duty cycles values for all three inverter legs are almost the same and around 50%. Sampling windows in the frame of both active vectors are not wide enough for reliable dc-link current measurement, so line current information could not be obtained. Fig. 15b shows a case of small amplitude reference voltage vector in the first SVPWM sector. Obviously, first signal *SAMP1* samples line current i_a, instead $-i_c$, while second sampling signal *SAMP2* measure zero value instead current i_a.

Fig. 16 shows results in case of applying original switching scheme without mechanism for obtaining minimal width of active voltage vectors. There is significant reconstructed current waveform distortion in critical intervals, which are useless for achieving vector control with only dc-link current feedback. Abrupt change and large deviation of reconstructed currents (i_a^{REC}, i_b^{REC}, i_c^{REC}) from actual current values (i_a, i_b, i_c) can be noticed in the area between different voltage sectors (*Sector*). To overcome these problems it is necessary to perform one of suggested mechanism for reliable dc-link current measurement by modifying the originally symmetrical PWM voltage patterns sufficiently, in the cases when longer active vectors are needed [6-9, 21].

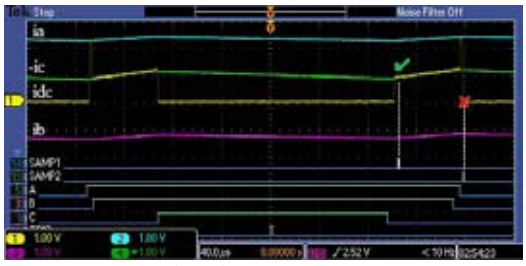

a) Passing from first into the second sector.

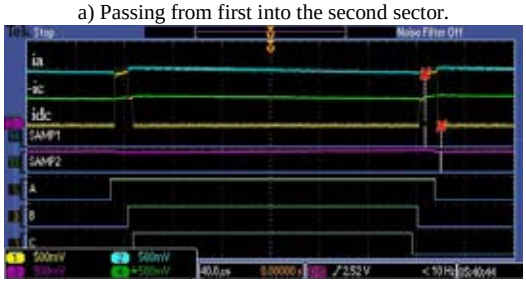

b) Small modulation index in sector 1.

Fig. 15. Critical cases for line current reconstruction method.

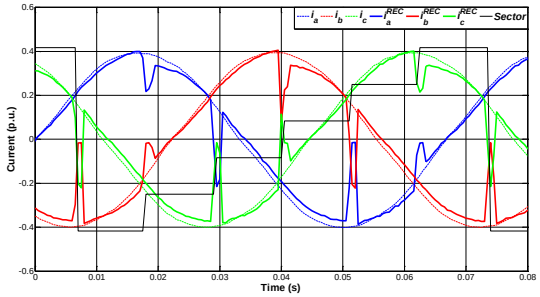

Fig. 16. Result of current reconstruction method without switching pattern modification.

Fig. 17 illustrates the applied solution principles with an example where small modulation index was referenced. PWM signals V_h *(A)*, V_m *(B)*, and V_l *(C)* does not form enough long active vectors for reliable dc-link current reading. Suggested method modifies PWM signals associated with the middle (V_m) and highest (V_h) voltage commands. Both signals are shifted in the right direction to form active vectors with minimal width T_{vector}^{MIN} for reliable dc-link current measurement. Firstly, if needed, PWM signal V_m is right–shifted by time:

$$\Delta T_{vector1} = T_{vector}^{MIN} - (T_m - T_l) \tag{15}$$

Active time intervals of PWM signal V_m during right (lagging) and left (leading) half-periods in PWM cycle should be updated to new values, T_{m2} and T_{m1}, respectively:

$$T_{m2} = T_h + \Delta T_{vector1}$$
$$T_{m1} = T_m - \Delta T_{vector1} \tag{16}$$

Then, second active vector duration has to be calculated and if needed, PWM signal V_h has to be right-shifted. Signal V_h width in lagging PWM half-period has to be extended, and in leading half-period to be reduced, to the new values T_{h2} and T_{h1}:

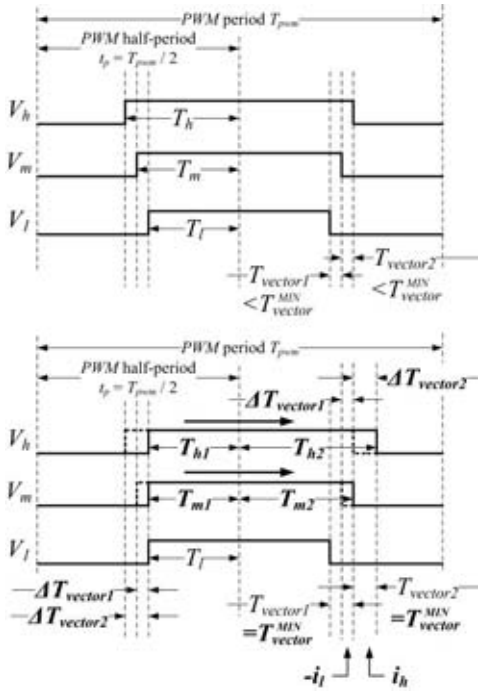

Fig. 17. PWM pattern modification principle used for reliable reconstruction.

$$\Delta T_{vector2} = T_{vector}^{MIN} - (T_h - T_{m2})$$
$$T_{h2} = T_h + \Delta T_{vector2} \quad (17)$$
$$T_{h1} = T_h - \Delta T_{vector2}$$

C. Test results

Figs. 18 and 19 illustrate the operation of conventional current reconstruction method with proposed modified switching pattern, in the closed-loop of described sensorless vector-control structure. Fig. 18 shows dynamic response of motor speed and stator dq-currents for same reference and operating conditions: ω_r^{REF} = *0,1 – 0,4 p.u.* and T_{load} = *1,5 Nm*. There are significant oscillations observed in dq-current components which are not caused only by current ripple on switching frequency, but also due to the current reconstruction mechanism which samples dc-link current in two different instants during PWM period [12]. Its final result is appearance of third and sixth harmonics in dq-current components. Maximal amplitude of the third and sixth harmonics in d-current was 9,4% and in q-current 43,3% of referenced value which contributed to higher distortion and oscillations in motor line current, torque and speed shown in the Fig. 19.

VI. Sensorless Vector Control with Proposed Current Reconstruction Method

A. Proposed current reconstruction method

The basic idea suggested in this paper represents an improvement of the method proposed in [6], which used the line-currents measured in both halves of the naturally symmetrical PWM switching period. The method proposed in [6] is based on sampling of the dc-link current in the center of the active voltage vectors four times during one PWM period and calculation of the two available line-current values by averaging the samples from two matching vector pairs.

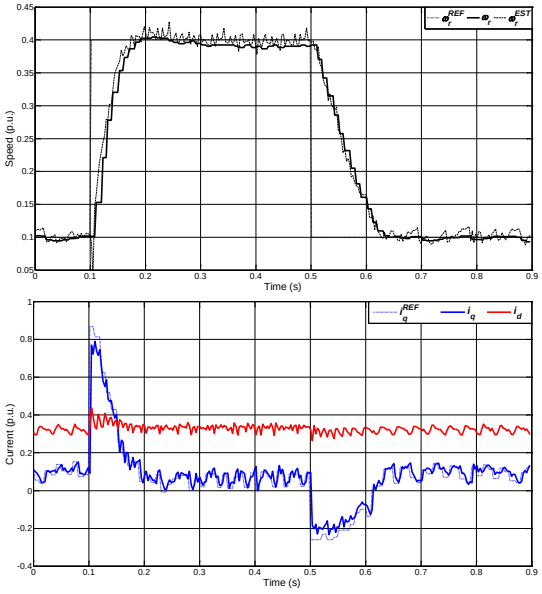

Fig. 18. DSP results: motor speed and dq-currents response for step reference ω_r^{REF} = *0,1 / 0,4 p.u.* – conventional current reconstruction method.

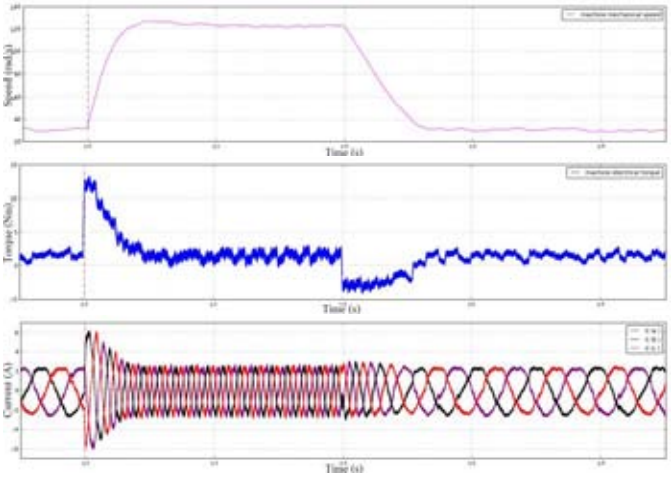

Fig. 19. HIL results: motor speed, torque and stator currents step response for ω_r^{REF}=*0,1-0,4 p.u.* – conventional current reconstruction method.

This approach provides synchronous measurement of all three line-currents, referred to the center of a PWM period. It effectively cancels error due to current ripple in the reconstructed line-currents and eliminates the current samples' mutual phase-shift. Besides its simplicity, this method is completely insensitive to machine parameter variances. However, in [6] the critical cases of a reference voltage vector passing between the six possible active vectors or with a low modulation index are neglected and not considered. The authors in [22] clearly emphasized that during these cases and with the PWM modified scheme used (where PWM signals are not symmetrical), the simultaneously sampled line-currents cannot be acquired. It clearly indicates there is a need to provide an improved procedure for reliably and more accurate measurement of the motor line-currents.

Considering the high PWM switching frequencies, up to 20 kHz, and usually employed electrical motors, one can conclude that there is no need for the very high current control-loop sampling rate at the PWM level. This fact allow us to record line-current information on the lagging (right) side of one PWM period and then on the leading (left) side of the subsequent PWM period and calculate the available line-currents by simple averaging of the corresponding recorded values. In this way, all three estimated line-currents would be referred to the same instant reflecting the average current value in two consecutive PWM periods. The proposed method enables us to improve the PWM pattern control in order to account for critical cases. It represents an extension of the modified PWM pattern explained in Section V.B where under critical conditions, the lagging half-pulse width is shifted to the right and the leading half-pulse width in the subsequent PWM period is shifted to the left in order to create sufficient sampling windows for current measurement (Fig. 21b).

Block diagram of implemented proposed control structure is illustrated in Fig. 20. Key blocks that improve control quality and performances are proposed current sampling block *F281X_IDC4*, *AVERAGING* block for finding inputs for conventional line current reconstruction *IABC_RECONS*, and

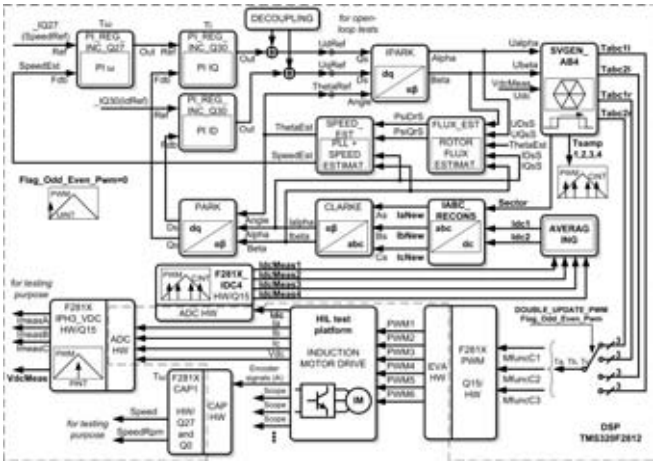

Fig. 20. DSP implementation of sensorless control structure for induction motor drive, with proposed current reconstruction algorithm (*F281X_IDC4+AVERAGING*) and modified modulator (*SVGEN_AB4*).

proposed modified voltage modulator *SVGEN_AB4* that overcomes critical cases in the reconstruction mechanism.

Fig. 21 shows the dc-link current and motor line currents during two consecutive PWM periods and details related to the proposed method. Sampling signals *SAMP1* and *SAMP4* are triggers for measurement of dc-link current in two consecutive PWM periods during matching active voltage vectors defined with only one inverter switch turned-on (here, with PWM signal *A*). *SAMP1* samples dc-link current at the beginning of the active voltage vector, and *SAMP4* at the end of the active vector. Similar, sampling signals *SAMP2* and *SAMP3* are triggers for measurement of dc-link current at the beginning and at the end of matching active voltage vectors defined with two upper switches turned-on (here, with PWM signals *A* and *B*), respectively.

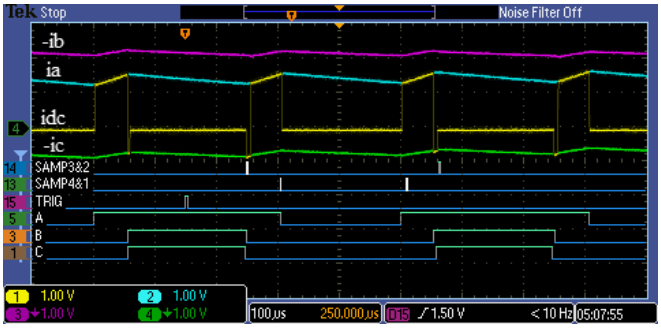

a) proposed sampling scheme with original symmetrical PWM pattern.

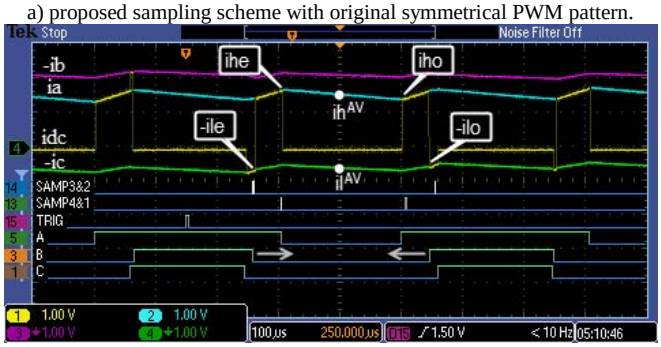

b) proposed sampling scheme and modified PWM pattern for improved line current reconstruction.

Fig. 21. Proposed current reconstruction method details.

The line currents at the time instant representing average values in two consecutive PWM periods, can be obtained using simple calculation:

$$i_l^{AV} = -\frac{i_{dc}(SAMP2)+i_{dc}(SAMP3)}{2} = -\frac{i_{lo}+i_{le}}{2}$$
$$i_h^{AV} = \frac{i_{dc}(SAMP1)+i_{dc}(SAMP4)}{2} = \frac{i_{ho}+i_{he}}{2} \quad (18)$$
$$i_m^{AV} = -\left(i_l^{AV}+i_h^{AV}\right)$$

It remains to assign the resultant currents i_h^{AV}, i_m^{AV} and i_l^{AV} to motor line-currents i_a, i_b and i_c depending on the actual sector number as in conventional case.

B. *Test results*

The first improvements in the reconstructed line-current waveform can be observed for a steady-state operation with ω_r^{REF} = *0,4 p.u.*, T_{load} = *1,5 Nm* and closed-loop operation with proposed current feedbacks, in Fig. 22. Fig. 22a shows actual (measured) line current values, i_a, i_b, and i_c, compared to the reconstructed line currents by proposed scheme, i_a^{NEW}, i_b^{NEW}, and i_c^{NEW}, and by conventional scheme, i_a^{REC} (only phase-*a* current is shown for clarity). Improved reconstructed currents do not include characteristic abrupt changes in its waveforms due to the passing reference voltage vector between SVPWM sectors. Proposed current reconstruction reduces presence of third and sixth harmonic terms in dq-current components by factor of 3, but also the offset from actual values which are noticeable especially in d-current component (Fig. 22b).

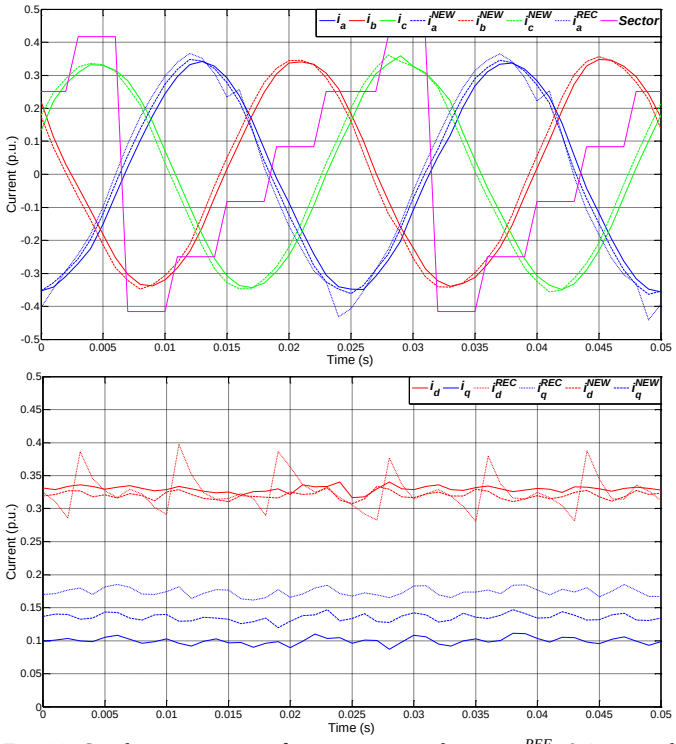

Fig. 22. Steady-state response for operating conditions ω_r^{REF}=*0,4 p.u.* and T_{load}=*1,5 Nm*: a) actual and reconstructed line currents; b) actual and reconstructed dq-currents with proposed (^{NEW}) and conventional reconstruction method (^{REC}).

This can be observed in motor torque and speed, not only in the steady-state, but also in transient intervals, where dynamic response is more stable. Figs. 23 and 24 show dynamic response of motor speed, electromagnetic torque and line currents in the same operating conditions: ω_r^{REF} = *0,1-0,4 p.u.* and T_{load} = *1,5 Nm*. Oscillations are less reduced for low speed reference *0,1 p.u.* because there are more frequent requirements for application of asymmetrical PWM signals due to the low reference voltage amplitude. However, obtained results together with the results in Fig. 18 verify that proposed method provide more stable stationary and dynamic response compared to the conventional current reconstruction method. Proposed control scheme shows almost the same behavior as in the case when direct measured line currents were used (Figs. 11 and 12).

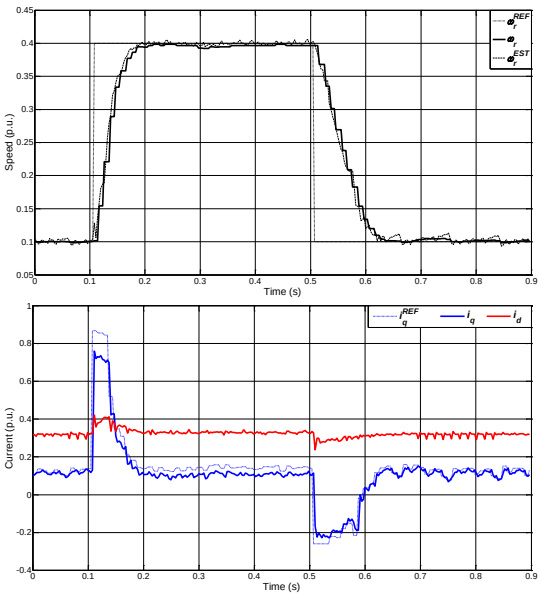

Fig. 23. DSP results: motor speed and dq-currents response for step reference ω_r^{REF} = *0,1 - 0,4 p.u.* – proposed current reconstruction method.

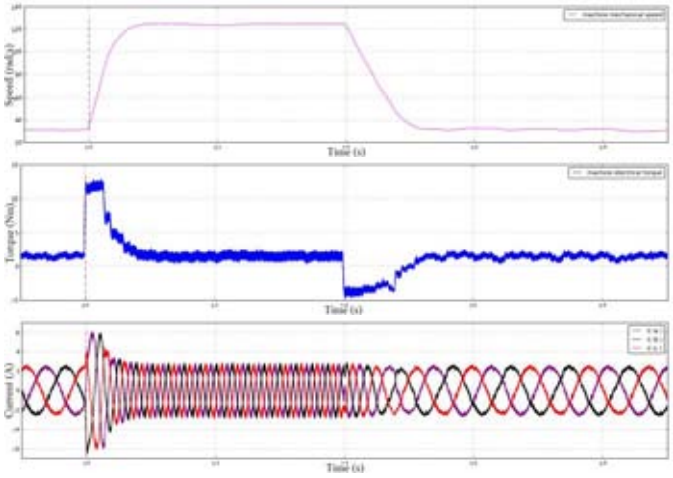

Fig. 24. HIL results: motor speed, torque and stator currents step response for ω_r^{REF}=*0,1-0,4 p.u.* – proposed current reconstruction method.

VII. Conclusion

Application of conventional line currents reconstruction method does not provide acceptable control quality and drive performance. The source of the problem is the distortion of the reconstructed motor currents. Distortion is caused by the nature of the employed method which samples dc-link current in different time instants related to the center of PWM period. Distortion in original abc-domain is reflected in the field-oriented reference frame dq-current components, which are further propagated through complete sensorless control structure. Results are increased oscillations in developed motor torque and speed, which can even cause unstable motor operation during transients.

Proposed solution of this problem does not use standard approach which introduces current filter blocks in the feedback path reducing the dynamic of complete control system. It is also completely independent on the machine model and parameters. It uses averaging of totally four dc-link current samples in two consecutive PWM periods, which significantly reduces the phase error and characteristic third and sixth harmonics in dq-current components. Average dc-link samples are referred to the same time instant which yields to the reconstructed current waveforms which are almost the same as actual measured values.

This paper verifies that proposed method reduces motor torque and speed oscillations to the acceptable level in the case when minimum number of sensors is used, and in conditions where all controller and estimator parameters are set for high-performance response. In future work proposed current reconstruction algorithm will be tested in various shaft-sensorless control structures.

Appendix

TABLE II
Controller Parameters

Symbol	Quantity	Value
f_{pwm}	PWM frequency	2 kHz
T_i	Current loop sampling period	1 ms
T_ω	Speed loop sampling period	10 ms
I_b	Current base value	7,02 A
U_b	Voltage base value	842,55 V
f_b	Frequency base value	100 Hz
ω_b	Angular frequency base value	628,32 rad/s
λ	Current loop dynamic parameter	300
K_{pi}	Current loop proportional gain	0,1357
K_{ii}	Current loop integral gain	0,0403
$K_{p\omega}$	Speed loop proportional gain	8,5716
$K_{i\omega}$	Speed loop integral gain	1,4851
i_q^{MAX}	Speed controller output positive limit	0,82 p.u. (1,45·I_n)
i_q^{MIN}	Speed controller output negative limit	-0,25 p.u.
K_{pf}	Flux compensator proportional gain	0,05
K_{if}^z	Flux compensator integral gain	0,00111
ω_{bw}	PLL filter bandwidth	300 Hz
K_{pp}	PLL filter proportional gain	26,657
K_{ip}^z	PLL filter integral gain	0,225

ACKNOWLEDGMENT

This research was partially co-funded by the Ministry of Education, Science and Technological Development of Republic of Serbia under contract No. III 042004 and by the Provincial Secretariat for Science and Technological Development of AP Vojvodina under contract No. 114-451-3508/2013-04.

REFERENCES

[1] N. Mohan, *Power Electronics and Drives*. Minneapolis: MNPERE, 2003, ch. 1.

[2] J. Holtz, "An approach to graphs of linear forms (Unpublished work style)," *Proc. of IEEE*, vol. 90, no. 8, pp. 1359-1394, Aug. 2002.

[3] C. Lascu, I. Boldea, F. Blaabjerg, "A Class of Speed-Sensorless Sliding-Mode Observers for High-Performance Induction Motor Drives," *IEEE Trans. on Ind. Electron.*, vol. 56, no. 9, Sept. 2009.

[4] T. G. Habetler, K. D. Hurst, "Sensorless Speed Measurement Using Current Harmonic Spectral Estimation in Induction Machine Drives," *IEEE Ind. Appl. Soc. Ann. Meet.*, pp. 553-559, 1995.

[5] P. Vas, *Sensorless Vector and Direct Torque Control*. New York: Oxford University Press, Inc., 1998.

[6] F. Blaabjerg, J. K. Pedersen, U. Jaeger, P. Thoegersen, "Single Current Sensor Technique in the DC Link of Three-Phase PWM-VS Inverters: A Review and a Novel Solution," *IEEE Trans. Ind. Appl.*, vol. 33, no. 5, pp. 1241-1253, Sept./Oct. 1997.

[7] H. Kim, T. M. Jahns, "Phase Current Reconstruction for AC Motor Drives Using a DC Link Single Current Sensor and Measurement Voltage Vectors," *IEEE Trans. Power Electron.*, vol. 21, no. 5, pp. 1413-1419, Sept. 2006.

[8] J. I. Ha, "Voltage Injection Method for Three-Phase Current Reconstruction in PWM Inverters Using a Single Sensor," *IEEE Trans. on Power Electron.*, vol. 24, no. 3, Mar. 2009.

[9] Y. Gu, F. Ni, D. Yang, H. Liu, "Switching-State Phase Shift Method for Three-Phase-Current Reconstruction With a Single DC-Link Current Sensor," *IEEE Trans. on Ind. Electron.*, vol. 58, no. 11, Nov. 2011.

[10] C. Zhang, F. Lin, "A Single Current Sensor Control Technique for Induction Motors," *Proc. Of PowerCon 2002*, vol. 4, pp. 2290-2293, 2002.

[11] A. Emadi, Y. J. Lee, K. Rajashekara, "Power Electronics and Motor Drives in Electric, Hybrid Electric, and Plug-In Hybrid Electric Vehicles," *IEEE Trans. Ind. Electron.*, vol. 55, no. 6, pp. 2237-2245, June 2008.

[12] D. Marcetic, E. Adzic, "Improved Three-Phase Current Reconstruction for Induction Motor Drives With DC-Link Shunt," *IEEE Ind. Electron.*, vol. 57, no. 7, pp. 2454-2462, July 2010.

[13] D. Majstorović, I. Čelanović, N. Teslić, N. Čelanović, V. A. Katić, "Ultra-Low Latency Hardware-in-the-Loop Platform for Rapid Validation of Power Electronics Designs," *IEEE Trans. Ind. Electron.*, vol. 58, no. 10, pp. 4708-4716, Oct. 2011.

[14] N. P. Quang, J.-A. Dittrich, *Vector Control of Three-Phase AC Machines*. Berlin: Springer, 2008.

[15] M. R. Stojić, *Digitalni sistemi upravljanja*. Beograd: Akademska misao, 2004.

[16] S. N. Vukosavić, *Digital Control of Electrical Drives*. New York: Springer Science, 2007.

[17] C. Lascu, I. Boldea, F. Blaabjerg, "A Modified Direct Torque Control for Induction Motor Sensorless Drive," *IEEE Trans. on Ind. Electron.*, vol. 36, no. 1, Jan./Feb. 2000.

[18] M. Comanescu, L. Xu, "An improved flux observer based on PLL frequency estimator for sensorless vector control of induction motors," *IEEE Trans. on Ind. Electron.*, vol. 53, no. 1, pp. 50-56, 2006.

[19] E. M. Adžić, M. S. Adžić, V. A. Katić, "Improved PLL for Power Generation Systems Operating under Real Grid Conditions," *Electronics*, vol. 15, no. 2, pp. 5-12, Dec. 2011.

[20] T. C. Green, B. W. Williams, "Derivation of motor line-current waveforms from the DC-link of an inverter," *Proc. Inst. Elect. Eng. B – Elect. Power Appl.*, vol. 136, no. 4, pp. 196-204, Jul. 1989.

[21] G. Liu, A. Kurnia, R. D. Larminat, "Procedure for measuring the current in each phase of a three-phase device via single current sensor," U.S. Patent 6 735 537, May 11, 2004.

[22] W. C. Lee, T. K. Lee, D. S. Hyun, "Comparison of Single-Sensor Current Control in the DC-Link for Three-Phase Voltage-Source PWM Converters," *IEEE Trans. Ind. Electron.*, vol. 48, no. 3, pp. 491-505, Jun 2001.